RESEARCH ARTICLE SUMMARY

NEUROSCIENCE

Ultrafast neuronal imaging of dopamine dynamics with designed genetically encoded sensors

Tommaso Patriarchi*, Jounhong Ryan Cho*, Katharina Merten, Mark W. Howe, Aaron Marley, Wei-Hong Xiong, Robert W. Folk, Gerard Joey Broussard, Ruqiang Liang, Min Jee Jang, Haining Zhong, Daniel Dombeck, Mark von Zastrow, Axel Nimmerjahn, Viviana Gradinaru, John T. Williams, Lin Tian†

INTRODUCTION: Neuromodulators, such as dopamine, norepinephrine, or serotonin, exert powerful control over neural circuit dynamics that give rise to diverse neural function and behavior. Altered neuromodulator signaling is a key feature of virtually all human neurological and psychiatric disorders, including Parkinson's disease, schizophrenia, depression, and addiction. Hence, drugs that mimic or block neuromodulators have become important components in the treatment of these disorders. Much work is devoted to determining exactly what information neuromodulatory neurons represent, but very little is known about how these signals alter the function of their target circuits.

RATIONALE: To address this problem, scientists need to be able to monitor the spatiotemporal dynamics of neuromodulatory signals in target circuits while also measuring and manipulating the elements of the circuit during natural behavior. However, existing technologies for detecting neuromodulators, such as analytic chemical or cell-based approaches, have limited spatial or temporal resolution, thus preventing high-resolution measurement of neuromodulator release in behaving animals. We recognized the potential of combining genetically encoded indicators based on fluorescent proteins with modern microscopy to support direct and specific measurement of diverse types of neuromodulators with needed spatial and temporal resolution.

RESULTS: We report the development and validation of dLight1, a novel suite of intensity-based genetically encoded dopamine indicators that enables ultrafast optical recording of neuronal dopamine dynamics in behaving mice. dLight1 works by directly coupling the conformational changes of an inert human dopamine receptor to changes in the fluorescence intensity of a circularly permuted green fluorescent protein. The high sensitivity and temporal resolution of dLight1 permit robust detection of physiologically or behaviorally relevant dopamine transients. In acute striatum slices, dLight1 faithfully and directly reports the time course and concentration of local dopamine release evoked by electrical stimuli, as well as drug-dependent modulatory effects on dopamine release. In freely moving mice, dLight1 permits deep-brain recording of dopamine dynamics simultaneously with optogenetic stimulation or calcium imaging of local neuronal activity. We were also able to use dLight1 to chronically measure learning-induced dynamic changes within dopamine transients in the nucleus accumbens at subsecond resolution. Finally, we show that two-photon imaging with dLight1 revealed a high-resolution (cellular level) dopamine transient map of the cortex showing spatially distributed, functionally heterogeneous dopamine signals during a visuomotor learning task.

ON OUR WEBSITE

Read the full article at http://dx.doi.org/10.1126/science.aat4422

CONCLUSION: To overcome the major barriers of current methods and permit high-resolution imaging of dopamine dynamics in the mammalian brain, we developed and applied a new class of genetically encoded indicators. This work validates our sensor design platform, which could also be applied to developing sensors for other neuromodulators, including norepinephrine, serotonin, melatonin, and opioid neuropeptides. In combination with calcium imaging and optogenetics, our sensors are well poised to permit direct functional analysis of how the spatiotemporal coding of neuromodulatory signaling mediates the plasticity and function of target circuits. ■

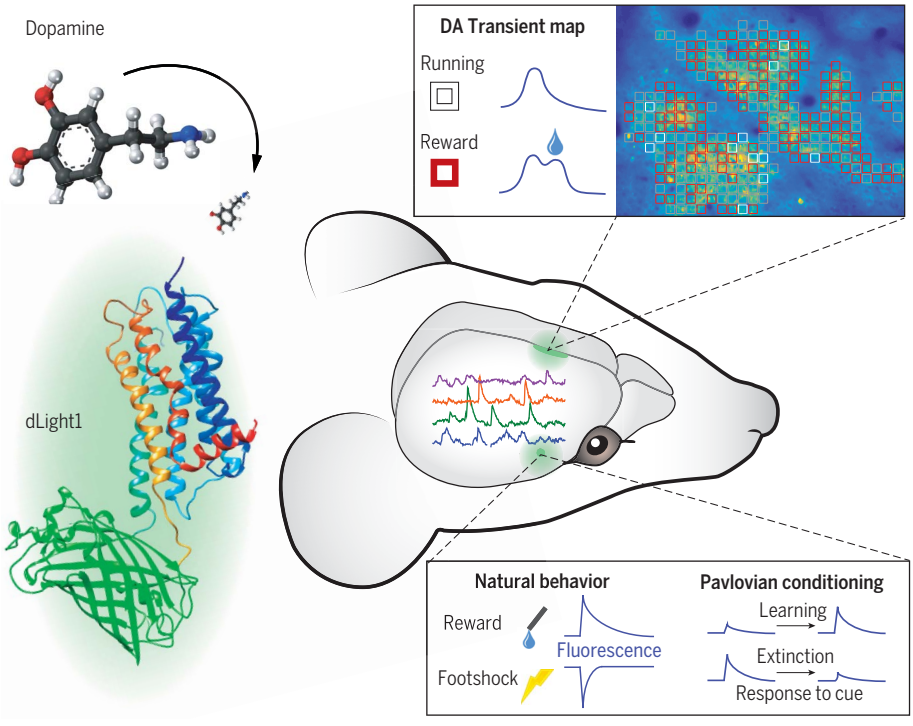

High-resolution dopamine imaging in vivo. dLight1 permits robust detection of physiologically and behaviorally relevant dopamine (DA) transients with high sensitivity and spatiotemporal resolution, including dynamic learning-induced dopamine changes in the nucleus accumbens (bottom) and task-specific dopamine transients in the cortex (top).

The list of author affiliations is available in the full article online.
*These authors contributed equally to this work.
†Corresponding author. Email: lintian@ucdavis.edu
Cite this article as T. Patriarchi *et al.*, *Science* **360**, eaat4422 (2018). DOI: 10.1126/science.aat4422

RESEARCH ARTICLE

NEUROSCIENCE

Ultrafast neuronal imaging of dopamine dynamics with designed genetically encoded sensors

Tommaso Patriarchi[1]*, Jounhong Ryan Cho[2]*, Katharina Merten[3], Mark W. Howe[4]†, Aaron Marley[5], Wei-Hong Xiong[6], Robert W. Folk[3], Gerard Joey Broussard[1], Ruqiang Liang[1], Min Jee Jang[2], Haining Zhong[6], Daniel Dombeck[4], Mark von Zastrow[5], Axel Nimmerjahn[3], Viviana Gradinaru[2], John T. Williams[6], Lin Tian[1]‡

Neuromodulatory systems exert profound influences on brain function. Understanding how these systems modify the operating mode of target circuits requires spatiotemporally precise measurement of neuromodulator release. We developed dLight1, an intensity-based genetically encoded dopamine indicator, to enable optical recording of dopamine dynamics with high spatiotemporal resolution in behaving mice. We demonstrated the utility of dLight1 by imaging dopamine dynamics simultaneously with pharmacological manipulation, electrophysiological or optogenetic stimulation, and calcium imaging of local neuronal activity. dLight1 enabled chronic tracking of learning-induced changes in millisecond dopamine transients in mouse striatum. Further, we used dLight1 to image spatially distinct, functionally heterogeneous dopamine transients relevant to learning and motor control in mouse cortex. We also validated our sensor design platform for developing norepinephrine, serotonin, melatonin, and opioid neuropeptide indicators.

Animal behavior is influenced by the release of neuromodulators such as dopamine (DA), which signal behavioral variables that are relevant to the functioning of circuits brainwide. Projections from dopaminergic nuclei to the striatum and cortex, for example, play important roles in reinforcement learning, decision-making, and motor control. Loss of DA or dysfunction of its target circuits has been linked to disorders such as Parkinson's disease, schizophrenia, and addiction (*1*–*3*).

Much work has been devoted to determining how neural representations of behavioral states are encoded in the firing patterns of neuromodulatory neurons (*4*–*9*), but very little is known about how the precise release of neuromodulators alters the function of their target circuits (*10*, *11*). To address this problem, an essential step is to monitor the spatiotemporal dynamics of neuromodulatory signals in target circuits while also measuring and manipulating the elements of the circuit during behavior.

Analytical techniques such as microdialysis and electrochemical microsensors have provided useful insights about neuromodulator presence (*12*, *13*) but suffer from poor spatial and/or temporal resolution and cannot be targeted to cells of interest. Optical approaches such as injected cell-based systems (CNiFERs) (*14*) and reporter gene–based iTango (*15*) can reveal DA release with high molecular specificity. However, these systems are limited by poor temporal resolution (seconds to hours), preventing direct detection of DA release events that occur on a subsecond time scale (*16*, *17*).

High-quality single fluorescence protein (FP)–based sensors that report calcium or glutamate transients with subsecond temporal resolution have recently been developed and are widely used (*18*, *19*). Here, we report the development of a set of single FP–based DA sensors, named dLight1, that enables imaging of DA transients with high spatiotemporal resolution in behaving animals.

Sensor engineering

Sensitive optical readout of changes in DA concentration was achieved by directly coupling the DA binding–induced conformational changes in human DA receptors to changes in the fluorescence intensity of circularly permuted green fluorescent protein (cpGFP). We did this by replacing the third intracellular loop (IL3) of the human dopamine D1 receptor (DRD1), D2 receptor (DRD2), and D4 receptor (DRD4) with a cpGFP module from the genetically encoded calcium indicator GCaMP6 (Fig. 1A).

To determine the insertion site of cpGFP in IL3 that produces maximal coupling of ligand-induced conformational changes to cpGFP fluorescence, we aligned the sequences of DRD1 and DRD4 with that of the β_2 adrenergic receptor (B2AR) (Fig. 1B), for which both active and inactive structure are available (*20*). The initial variant, obtained by inserting a cpGFP module with original linker sequences (LSSLE-cpGFP-LPDQL) between Lys^{232} and Lys^{269} of DRD1, was well expressed at the plasma membrane of human embryonic kidney (HEK293) cells and showed a fluorescence decrease ($\Delta F/F_{max}$ = −19.4 ± 0.02%) in response to puffed DA (fig. S1A). To obtain a positive-response sensor, we screened a library of 585 variants in HEK cells (Fig. 1C and fig. S1B). The variant with the largest positive fluorescence response (max $\Delta F/F_{max}$ = 230 ± 9%) and excellent membrane localization was named dLight1.1 (Fig. 1D). In situ DA titration on HEK cells revealed submicromolar apparent affinity of dLight1.1 (affinity constant K_d = 330 ± 30 nM; Fig. 1E).

We next sought to further tune the dynamic range and affinity of the sensor. Mutation of Phe^{129}, a highly conserved residue among many G protein–coupled receptors (GPCRs) (*21*), into Ala (dLight1.2) slightly increased dynamic range (max $\Delta F/F_{max}$ = 340 ± 20%, K_d = 770 ± 10 nM; Fig. 1, D and E). Optimizing the cpGFP insertion site in dLight1.1 and dLight1.2 (fig. S1, C to G) greatly increased the dynamic range but also reduced the affinity to micromolar range (dLight1.3a: $\Delta F/F_{max}$ = 660 ± 30%, K_d = 2300 ± 20 nM, fig. S2, A and B; dLight1.3b: $\Delta F/F_{max}$ = 930 ± 30%, K_d = 1680 ± 10 nM; Fig. 1, D and E). Insertion of the cpGFP module into DRD4 and DRD2 produced dLight1.4 and dLight1.5, respectively, which exhibited nanomolar affinity with a relatively small dynamic range [dLight1.4: $\Delta F/F_{max}$ = 170 ± 10%, K_d = 4.1 ± 0.2 nM, Fig. 1, B, D, and E; dLight1.5: DA, $\Delta F/F_{max}$ = 180 ± 10%, K_d = 110 ± 10 nM; quinpirole (synthetic agonist of D2 dopamine receptors), $\Delta F/F_{max}$ = 124 ± 19%, fig. S2, A to C]. In addition, we engineered a control sensor by incorporating a D103A mutation in dLight1.1 to abolish DA binding (control sensor: $\Delta F/F$ = 0.4 ± 4%, Fig. 1E) (*22*). Because dLight1.1 and dLight1.2 produced large responses at low DA concentration (e.g., 100 nM) without approaching response saturation (Fig. 1E, inset) and had submicromolar affinity, we further characterized these two sensors.

Sensor characterization

These two sensors showed peak emissions at 516 nm and 920 nm for one- and two-photon illumination in HEK cells, respectively (fig. S3). In situ titration on dissociated hippocampal neurons and on HEK293 cells showed similar apparent affinities to DA (Fig. 1E and fig. S4, A to C). Single 5-ms pulses of uncaged DA were robustly detected on the dendrites of cultured neurons, and the fluorescence response tracked uncaging pulse duration (fig. S4, D to F). In cultured

[1]Department of Biochemistry and Molecular Medicine, University of California, Davis, 2700 Stockton Boulevard, Sacramento, CA 95817, USA. [2]Division of Biology and Biological Engineering, California Institute of Technology, Pasadena, CA 91125, USA. [3]Waitt Advanced Biophotonics Center, Salk Institute for Biological Studies, La Jolla, CA 92037, USA. [4]Department of Neurobiology, Northwestern University, Evanston, IL 60208, USA. [5]Department of Cellular and Molecular Pharmacology, University of California, San Francisco, CA 94131, USA. [6]Vollum Institute, Oregon Health & Science University, Portland, OR 97239, USA.
*These authors contributed equally to this work.
†Present address: Department of Psychological and Brain Sciences, Boston University, Boston, MA 02215, USA.
‡Corresponding author. Email: lintian@ucdavis.edu

hippocampal slices, dLight1 could reliably detect submicromolar DA concentration changes at dendrites and single dendritic spines (fig. S4, G to I).

We then investigated the endogenous and pharmacological molecular specificity of the sensor. dLight1 was less sensitive to norepinephrine and epinephrine than to DA by factors of ~70 and ~40, respectively; negligible responses were observed to all other neuromodulators tested (fig. S5). The amplitude of the response to each pharmacological compound reflected the efficacy of drugs on the wild-type receptors, with the largest response to the full agonist dihydrexidine ($\Delta F/F$ = 300 ± 10%), followed by partial agonists (Fig. 1F). The response to DA was abolished in the presence of the DRD1 antagonists SKF-83566 and SCH-23390 but was unaffected by the DRD2 antagonists haloperidol and sulpiride (Fig. 1F).

To investigate the possible interference of sensor expression with G protein signaling, we first measured the effect of sensor expression on the ligand-induced cyclic adenosine monophosphate (cAMP) response (fig. S6) (*23*). Transiently transfected dLight1.1 and dLight1.2 triggered no significant cAMP response in HEK cells, similar to the negative control (EGFP), whereas wild-type DRD1 receptor significantly did (fig. S6A). The conversion of DRD1 to a fluorescent sensor thus apparently blocked the scaffold's ability to bind G protein and trigger the signaling cascade. When introduced into a cell line that endogenously expressed DRD1 (U2OS), dLight1 did not significantly alter the dose-response curve for DA (P = 0.96, fig. S6B). dLight1 also showed a significant reduction in agonist-induced internalization, a readout of DRD1 engagement of β-arrestin (*24*), when compared to wild-type DRD1 (fig. S6C). Total internal reflectance fluorescence (TIRF) imaging verified that dLight1 remained diffusely distributed in the plasma membrane, without any detectable internalization, during a complete cycle of ligand-dependent fluorescence change (fig. S6, D to F). Taken together, these results indicate that the dLight sensors are suitable for use on the cell membrane without affecting endogenous signaling through G proteins or engagement of β-arrestins.

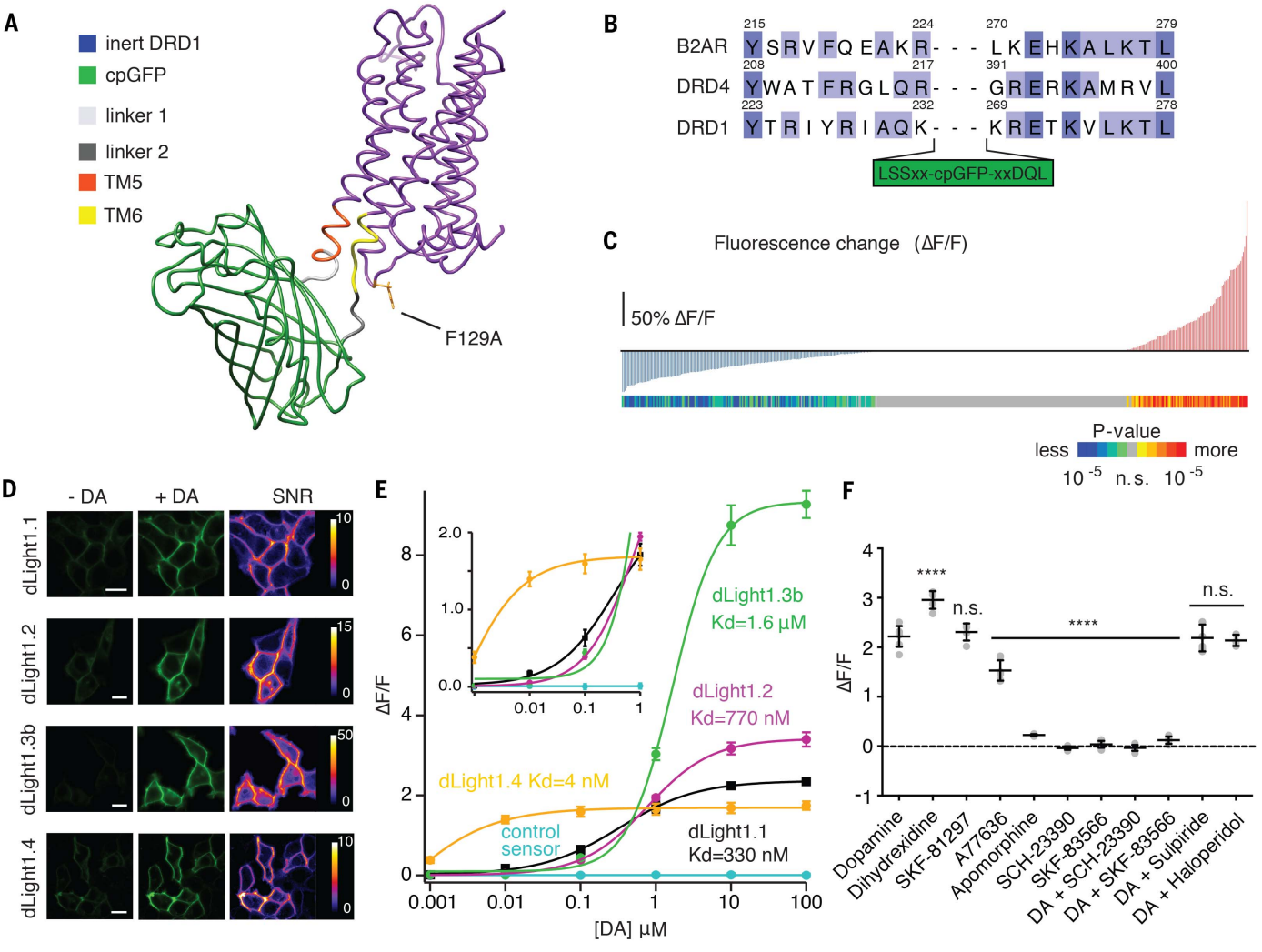

Fig. 1. Development and characterization of dLight1. (**A**) Simulated structure of dLight1 consisting of DRD1 and cpGFP module. (**B**) Sequence alignment of transmembrane (TM) domain 5 and 6 in β_2AR, DRD1, and DRD4. Library design is shown. Amino acid abbreviations: A, Ala; D, Asp; E, Glu; F, Phe; G, Gly; H, His; I, Ile; K, Lys; L, Leu; M, Met; Q, Gln; R, Arg; S, Ser; T, Thr; V, Val; W, Trp; Y, Tyr. (**C**) Screening result of 585 linker variants. Red and blue vertical bars indicate fluorescence changes ($\Delta F/F$) in response to 10 µM DA; significance values of $\Delta F/F$ are shown by colored bars and scale (n = 3 trials, two-tailed t test). (**D**) Expression of dLight variants in HEK cells. Fluorescence intensity and signal-to-noise ratio of apo and sat state are shown. Scale bars, 10 µm. (**E**) In situ titration of DA on HEK cells. Data were fitted with the Hill equation (n = 5). (**F**) Pharmacological specificity of dLight1.1. DRD1 full agonist (dihydrexidine, 295 ± 8%, n = 5); DRD1 partial agonists (SKF-81297, 230 ± 7.7%, n = 5; A77636, 153 ± 7.8%, n = 7; apomorphine, 22 ± 0.8%, n = 6); DRD1 antagonists (SCH-23390, −0.04 ± 0.01%, n = 7; SKF-83566, 0.04 ± 0.03%, n = 7); DRD2 antagonists (sulpiride, 213 ± 5.1%, n = 5; haloperidol, 219 ± 11%, n = 6). Data are means ± SEM. ****P < 0.0001 [one-way analysis of variance (ANOVA), Dunnett posttest]; n.s., not significant.

Versatile application to other neuromodulators

We next applied the design strategy of dLight1 to modularly develop a class of intensity-based sensors for various neuromodulators and neuropeptides. We selected a subset of GPCRs, including G_s-coupled β_1 and β_2 adrenergic receptors (B1AR and B2AR); G_i-coupled κ- and μ-type opioid receptors (KOR, MOR) and α_2 adrenergic receptor (A2AR); and G_q-coupled 5-hydroxytryptamine (serotonin) receptor-2A (5HT2A) and melatonin type-2 receptor (MT2). As with dLight1, we replaced IL3 with cpGFP, with insertion sites chosen to preserve the conserved positive charges (fig. S7A). All sensors localized to the membrane and showed positive fluorescence responses to their respective agonists (fig. S7B).

Two-photon imaging of DA release in dorsal striatum ex vivo and in vivo

We next used dLight1 to measure the time course and concentration of endogenous DA release triggered by electrical stimulation and drug

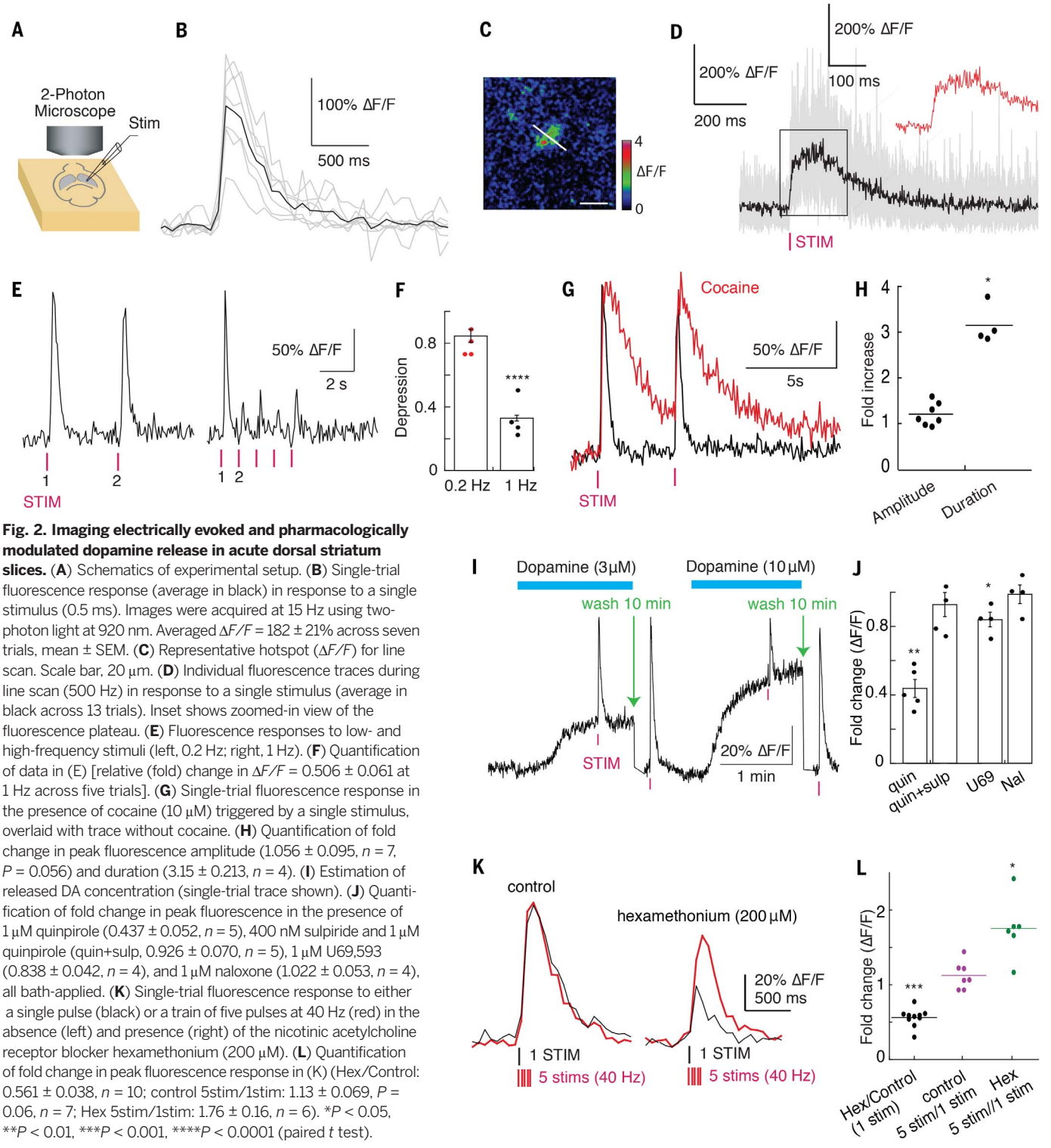

Fig. 2. Imaging electrically evoked and pharmacologically modulated dopamine release in acute dorsal striatum slices. (**A**) Schematics of experimental setup. (**B**) Single-trial fluorescence response (average in black) in response to a single stimulus (0.5 ms). Images were acquired at 15 Hz using two-photon light at 920 nm. Averaged $\Delta F/F$ = 182 ± 21% across seven trials, mean ± SEM. (**C**) Representative hotspot ($\Delta F/F$) for line scan. Scale bar, 20 μm. (**D**) Individual fluorescence traces during line scan (500 Hz) in response to a single stimulus (average in black across 13 trials). Inset shows zoomed-in view of the fluorescence plateau. (**E**) Fluorescence responses to low- and high-frequency stimuli (left, 0.2 Hz; right, 1 Hz). (**F**) Quantification of data in (E) [relative (fold) change in $\Delta F/F$ = 0.506 ± 0.061 at 1 Hz across five trials]. (**G**) Single-trial fluorescence response in the presence of cocaine (10 μM) triggered by a single stimulus, overlaid with trace without cocaine. (**H**) Quantification of fold change in peak fluorescence amplitude (1.056 ± 0.095, n = 7, P = 0.056) and duration (3.15 ± 0.213, n = 4). (**I**) Estimation of released DA concentration (single-trial trace shown). (**J**) Quantification of fold change in peak fluorescence in the presence of 1 μM quinpirole (0.437 ± 0.052, n = 5), 400 nM sulpiride and 1 μM quinpirole (quin+sulp, 0.926 ± 0.070, n = 5), 1 μM U69,593 (0.838 ± 0.042, n = 4), and 1 μM naloxone (1.022 ± 0.053, n = 4), all bath-applied. (**K**) Single-trial fluorescence response to either a single pulse (black) or a train of five pulses at 40 Hz (red) in the absence (left) and presence (right) of the nicotinic acetylcholine receptor blocker hexamethonium (200 μM). (**L**) Quantification of fold change in peak fluorescence response in (K) (Hex/Control: 0.561 ± 0.038, n = 10; control 5stim/1stim: 1.13 ± 0.069, P = 0.06, n = 7; Hex 5stim/1stim: 1.76 ± 0.16, n = 6). *P < 0.05, **P < 0.01, ***P < 0.001, ****P < 0.0001 (paired t test).

modification in acute striatal slices with two-photon imaging (Fig. 2A). Two to four weeks after injection of an adeno-associated virus encoding dLight1 (AAV9.*hSynapsin1*.dLight1.2) into the dorsal striatum, we observed both broadly distributed and localized fluorescence transients across the field of view (Fig. 2, B and C, and fig. S8, A to C) in response to a single electrical stimulus. Fast line scan at these hotspots (Fig. 2C) revealed a rapid onset of fluorescence increase (rise $\tau_{1/2}$ = 9.5 ± 1.1 ms) followed by a plateaued peak (averaged $\Delta F/F$ = 220 ± 50%) for about 150 ms, which decayed to baseline in about 400 ms (decay $\tau_{1/2}$ = 90 ± 11 ms, Fig. 2D). We observed robust and reproducible fluorescent transients to low-frequency stimuli over a prolonged imaging period, whereas subsequent higher-frequency stimuli elicited significantly smaller responses (Fig. 2, E and F), indicating strong depression from an initially high probability of release. Blockade of DA reuptake with cocaine significantly prolonged the decay of fluorescence from peak to baseline (Fig. 2, G and H), but with equivocal effect on response amplitude (Fig. 2, G and H). Application of the competitive antagonist SKF83566 eliminated the responses (fig. S8F), confirming that fluorescent signals are indeed attributable to DA binding.

We next used dLight1 to estimate released DA concentration induced by a brief electrical stimulus. By comparison with a concentration-response curve (fig. S8, D, E, and G), the fluorescence response suggested a DA release of 10 to 30 μM (Fig. 2I), which is one to two orders of magnitude higher than previously reported in ventral striatum using fast-scan cyclic voltammetry (FSCV) (*25*) and is similar to that reported by measuring DRD2 activation (*26*). Addition of saturating amphetamine (10 μM in the presence of 400 μM sulpiride) increased tonic DA to 3.3 μM (fig. S8, F and G).

We then examined the action of known modulators of DA release using dLight1 (Fig. 2, J to L). Activation of D2 autoreceptors with quinpirole decreased the electrically evoked fluorescence transients; this effect was significantly reversed by the application of sulpiride (Fig. 2J). Perfusion with a κ-opioid receptor agonist (U69,593) caused a small decrease in the amplitude, which was completely blocked by naloxone (Fig. 2J). We then imaged the effects of nicotinic receptor activation

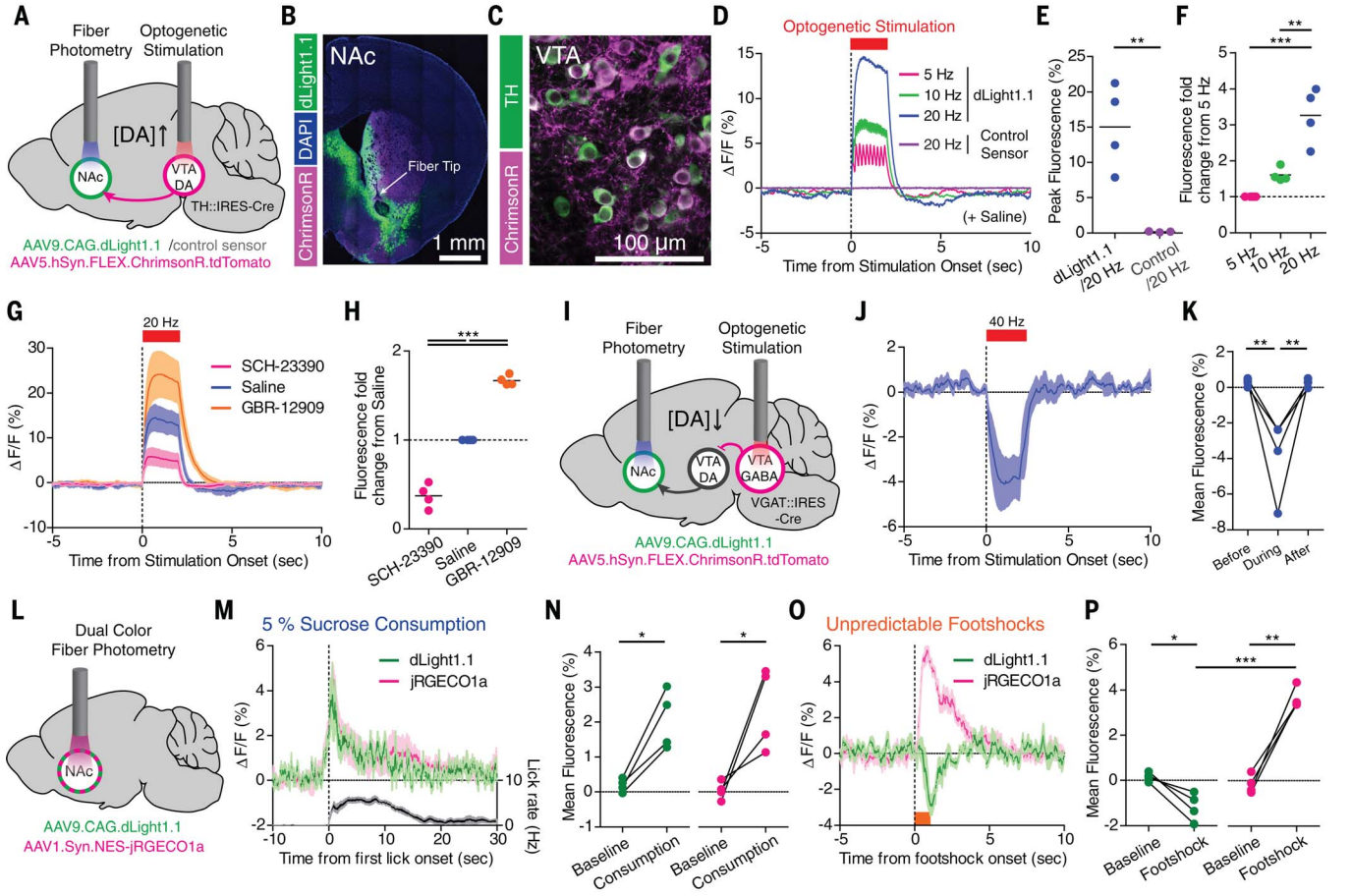

Fig. 3. Deep brain imaging of DA release triggered by optogenetic stimulation and combined with calcium imaging in freely behaving mice. (**A**) Schematics showing fiber photometry recording of dLight1.1 or control sensor in NAc while stimulating VTA DA neurons by optogenetics. (**B**) Expression of dLight1.1 in NAc around fiber tip location and ChrimsonR-expressing axons from midbrain. (**C**) ChrimsonR-expressing TH^+DA neurons in VTA. (**D**) Averaged fluorescence increase in response to optogenetic stimuli (n = 5 mice). (**E**) Quantification of peak fluorescence at 20 Hz. (**F**) Fluorescence fold changes relative to 5 Hz. (**G** and **H**) Optogenetically induced fluorescence increase of dLight1.1 after systemic administration of saline, D1 antagonist (SCH-23390, 0.25 mg/kg), and DA reuptake inhibitor (GBR-12909, 10 mg/kg) (n = 5 mice). (**I**) Schematics showing fiber photometry recording of dLight1.1 in NAc and optogenetic stimulation of VTA GABA neurons that inhibits VTA DA neurons. (**J** and **K**) Averaged fluorescence decrease in response to optogenetic stimulation at 40 Hz (n = 4 mice) and quantification of mean fluorescence. (**L**) Dual-color fiber photometry recording of DA release with dLight1.1 and local neuronal activity with jRGECO1a. (**M** and **N**) Increase of dLight1.1 (green) and jRGECO1a (magenta) fluorescence during 5% sucrose consumption with lick rate (black, n = 5 mice) and quantification of mean fluorescence. (**O** and **P**) Fluorescence decrease in dLight1.1 (green) and increase in jRGECO1a (magenta) during unpredictable footshock delivery (0.6 mA for 1 s, n = 5 mice) and quantification of mean fluorescence. Data shown are means ± SEM. *P < 0.05, **P < 0.01, ***P < 0.001 (paired or unpaired t tests for two-group comparisons; one-way ANOVA by post hoc Tukey test for multiple-group comparisons).

in mediating the probability of DA release. Blockade of nicotinic receptors with hexamethonium profoundly reduced the fluorescence transient, which depended on the number of stimuli (Fig. 2, K and L). In the absence of hexamethonium, the amplitude of the fluorescence remained consistent regardless of the stimulation protocol (Fig. 2, K and L) (*27*).

Next, we asked whether dLight1 could reliably report DA signals associated with mouse locomotion in dorsal striatum, which was labeled with AAV1.*hSynapsin1*.dLight1.1/1.2 and AAV1.*hSynapsin1*.flex.tdTomato. We measured DA transients with two-photon imaging during rest and self-initiated locomotion (fig. S9). Consistent with in vivo two-photon calcium imaging of substantia nigra pars compacta (SNc) axon terminals in dorsal striatum (*10*), dLight1 reliably showed

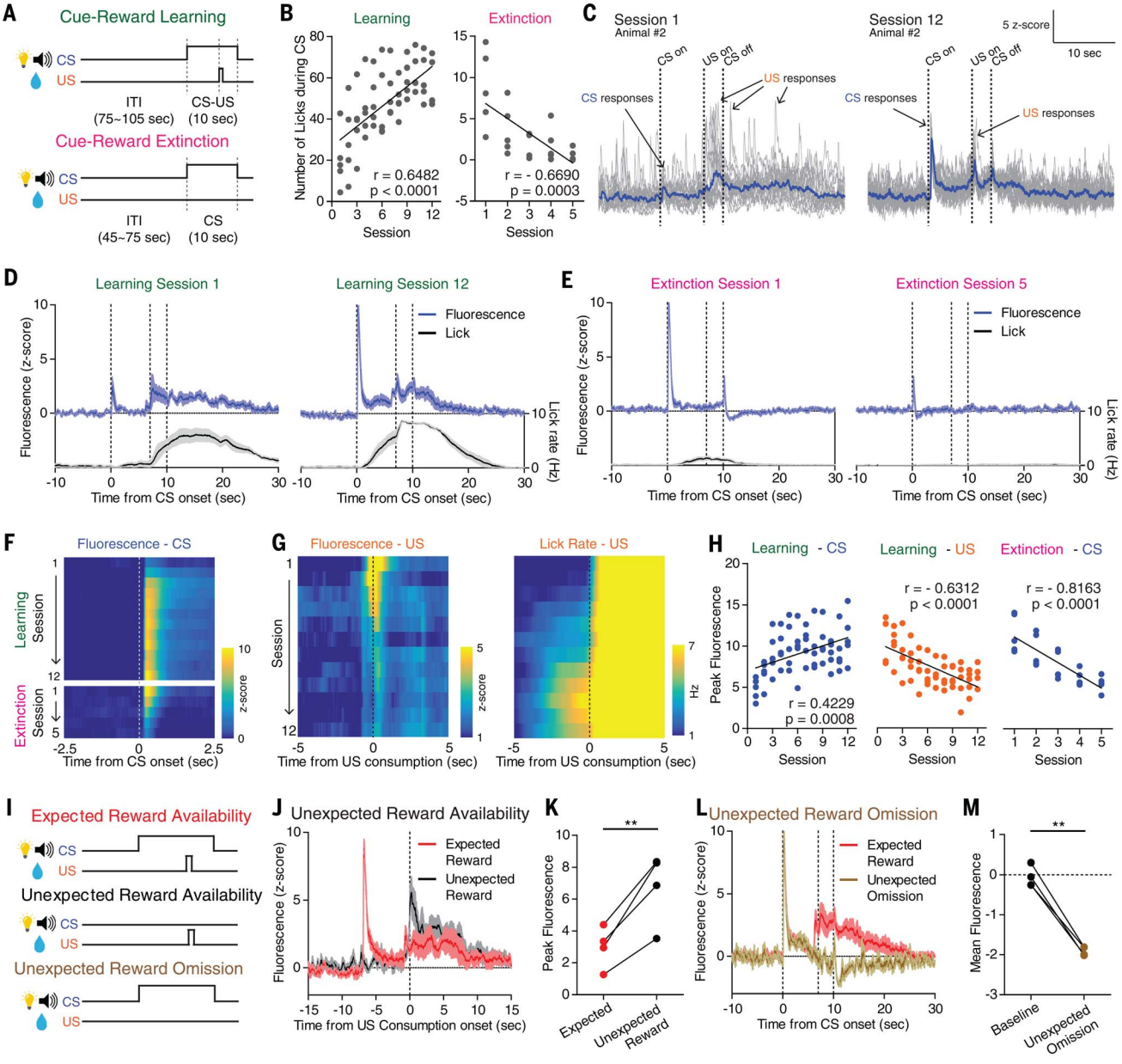

Fig. 4. Dynamic changes of NAc DA signaling during appetitive Pavlovian conditioning and reward prediction error. (**A**) Pavlovian conditioning procedures involved learning to associate neutral cues (CS; house light and 5-kHz tone) with a sucrose reward (US; 50 µl of 5% sucrose) and subsequent extinction. (**B**) Change of CS-evoked licks across cue-reward learning (left) and extinction (right). (**C** and **D**) dLight1.1 dynamics in response to CS and US in first and last sessions of cue-reward learning, shown in single (gray) and averaged (blue) trials (n = 20 trials) from a single animal (C) or averaged across all trials and animals (n = 5 mice) (D). Lick rate is shown in black. (**E**) Same as (D) for cue-reward extinction (n = 5 mice). In (D) and (E), dotted lines indicate CS onset, US onset, and CS offset, respectively. (**F** to **H**) Evolution of CS-evoked (F) and US-evoked [(G), left] average fluorescence and US-triggered licks [(G), right] across learning and extinction sessions. (H) Quantification of peak fluorescence across learning and extinction. (**I**) Reward prediction error procedure. (**J**) Fluorescence response during expected (red) versus unexpected (black) reward consumption (n = 4 mice). (**K**) Peak fluorescence evoked by expected (red) and unexpected (black) reward consumption. (**L**) Fluorescence response during expected (red) versus unexpected (brown) reward omission (n = 4 mice). Second and third dotted lines indicate US onset and CS offset, respectively. (**M**) Mean fluorescence during baseline and after unexpected reward omission. Data are means ± SEM. $^{**}P < 0.01$ (Pearson correlation coefficient and paired t test).

widespread and synchronous subsecond transients associated with spontaneous locomotion, which was clearly distinguishable from motion artifacts (fig. S9, A to E). The DA transients were rapidly and bidirectionally modulated with respect to locomotion. Accelerations were associated with an increase and decelerations with a decrease in fluorescence (peak mean cross-correlation 240 ms fig. S9, F to L).

In summary, dLight1 faithfully and directly reports the time course and concentration of local DA release and drug-dependent modulatory effects on DA release in an acute striatum slice. In addition, dLight1 enables direct visualization of locomotion-triggered DA release in behaving mice.

Deep-brain recording of DA dynamics simultaneously with optogenetics or calcium imaging

The nucleus accumbens (NAc) receives projections from dopaminergic neurons in the ventral tegmental area (VTA). To directly probe DA release in freely moving mice, we delivered AAV9.*CAG*.dLight1.1 or AAV9.*CAG*.control_sensor in NAc, followed by fiber photometry imaging (Fig. 3 and fig. S10, A and B). dLight1 revealed visible spontaneous DA transients, which were absent in the imaging sessions using the control sensor (fig. S10C).

To optically activate VTA dopaminergic neurons, we infected VTA of *TH*::IRES-Cre mice with AAV5.*hSynapsin1*.flex.ChrimsonR.tdTomato (*28*) (Fig. 3, A to C, fig. S11, A and B, and fig. S12, A and D). The high temporal resolution of dLight1 enabled detection of individual peaks of DA transients in response to 5-, 10-, and 20-Hz photostimulation (Fig. 3D and fig. S13, A to C). The amplitude of fluorescence increase was

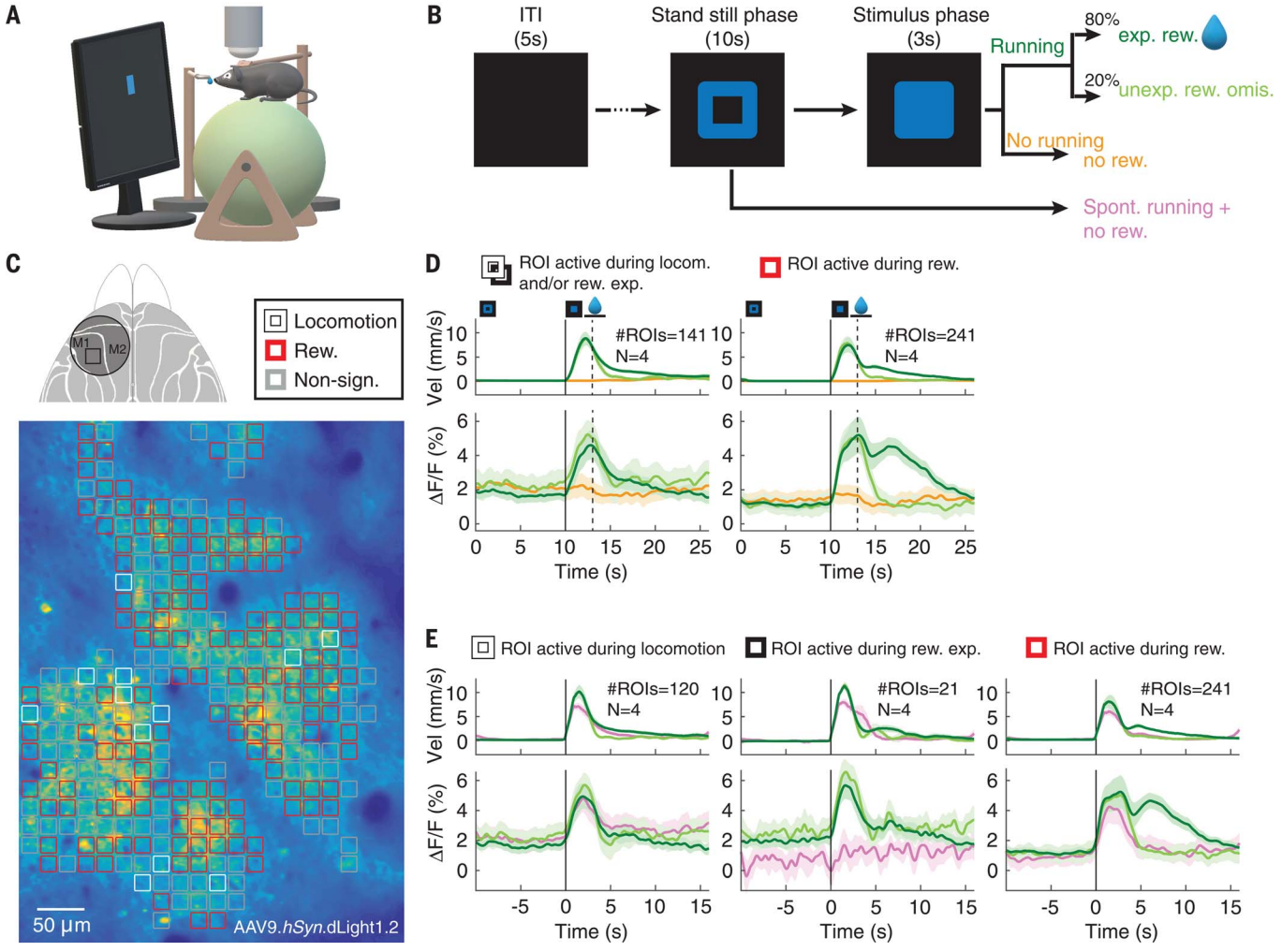

Fig. 5. Spatially resolved imaging of cortical dopamine release during a visuomotor association task. (**A**) Schematics of experimental setup. (**B**) A trial was initiated when mice were required to stand still for 10 s after a visual cue (blue square). If mice started to run during the stimulus phase ("hit trials"), a water reward was given. In 20% of randomly selected hit trials, the reward was withheld. If no run was triggered by stimulus presentation, the trials were counted as "miss trials." Erroneous or spontaneous runs during the standstill phase ended the trial (no "Go" cue or reward). (**C**) Top: Dorsal view of mouse cortex with the chronic cranial window (circle) and imaging location indicated (square). Bottom: Heat map of dLight1.2 expression pattern in layer 2/3 of M1 cortex. The image is overlaid with computationally defined regions of interest (ROIs, ~17 µm × 17 µm). Colored ROIs indicate the type of fluorescence responses observed during the task. (**D**) Population data (N = 4 mice, n = 19 recording sessions) showing average task-related dLight1.2 transients (bottom) and mouse running velocity (top) aligned to trial/standstill cue onset (0 s). The solid vertical line indicates "Go" cue onset. The dashed line marks the end of the reward expectation phase during unrewarded hit and miss trials. The period during which running velocity–dependent reward consumption occurred is indicated by the horizontal line. Left: ROIs showing significantly increased responses during reward expectation/locomotion. Right: ROIs showing significant fluorescence increases to reward (dark green) but not unexpected reward omission (light green). Shaded areas of $\Delta F/F$ traces indicate SD. (**E**) Population data realigned to running onset (vertical black line). ROIs with "Go" cue responses [(D), left] can be subdivided into ROIs responsive to locomotion in all trials (left) and responsive to reward expectation only (center), with no fluorescence increases during spontaneous runs (pink). $P < 0.05$ (Wilcoxon test, Bonferroni-corrected for multiple comparisons).

correlated with the frequency of photostimulation (Fig. 3, D and F). In contrast, no fluorescence changes were observed with the control sensor using 20-Hz stimuli (Fig. 3, D and E). Relative to saline-injected controls, systemic administration of SCH-23390 significantly reduced optogenetically induced dLight1 responses, whereas the reuptake inhibitor GBR-12909 enhanced them (Fig. 3, G and H).

Next, we examined whether dLight1 can report inhibition of DA transients. To induce transient inhibition of VTA dopaminergic neurons, we optogenetically stimulated VTA γ-aminobutyric acid–releasing (GABAergic) neurons in *VGAT*::IRES-Cre mice (*29*) (Fig. 3I). Histology confirmed ChrimsonR expression in VTA GABAergic neurons (fig. S12, B, C, and E). We observed rapid and reversible reductions in dLight1 fluorescence in response to VTA GABAergic neuron photoactivation at 40 Hz (Fig. 3, J and K, and fig. S13D), indicating that dLight1 can report bidirectional changes in local DA release.

Motivationally salient stimuli modify DA neuron firing and downstream NAc activity (*9*, *29*, *30*). To link the DA release to local neuronal activity, we performed dual-color measurements with dLight1 and the red-shifted calcium indicator jRGECO1a (*31*) in lateral core/shell regions (Fig. 3L and figs. S10B, S11A, and S12F). When mice voluntarily consumed a reward (50 μl of 5% sucrose), we observed a concordant increase of DA concentration and local population activity (Fig. 3, M and N, and fig. S13E), similar to a class of NAc single units showing excitation upon reward (*32*). In contrast, footshocks suppressed DA release while enhancing local neuronal activity, indicating dissociation between DA dynamics and local circuit activity (Fig. 3, O and P, and fig. S13F).

Chronic imaging of DA dynamics throughout cue-reward learning

We next examined the utility of dLight1 in reporting modulation of DA signaling in response to conditioned stimuli (CS) and unconditioned stimuli (US) throughout Pavlovian conditioning (Fig. 4A) (*8*, *33*, *34*). Mice successfully learned to associate the predictive cues to the reward, as shown by increasing numbers of licks during CS over the course of training and by decreasing numbers of licks during extinction learning (Fig. 4B).

Repeated fiber photometry recordings in NAc revealed two types of DA transients modulated during associative learning: increased DA response to the predictive cues and decreased response to reward consumption across sessions. In the first session, a small and time-locked phasic DA signal was present at the CS onset, whereas after US the DA signal was larger and also more temporally spread (Fig. 4, C and D), consistent with US consumption onsets being highly variable at early stages (fig. S14, A and B). Aligning to consumption onset revealed large DA signal to the US at the first session (Fig. 4C and fig. S14A). Upon repeated cue-reward pairings, the amplitude of CS response significantly increased (Fig. 4, C, D, F, and H, and fig. S14C). On the other hand, US response, when aligned to the consumption onset, showed a monotonic decrease across learning sessions (Fig. 4, G and H, and fig. S14D) (*9*, *33*). During extinction, we observed an attenuated phasic CS response (Fig. 4, E, F, and H). The amplitude of the phasic CS response was correlated with CS-triggered licking behavior during both learning and extinction sessions (fig. S14E).

We further investigated whether dLight1 can report signals correlated with "reward prediction error" (*4*). After the animals had fully learned CS-US association, mice underwent "unexpected reward availability" sessions (in which the US was occasionally made available without the CS) between normal paired trials (Fig. 4I). Unexpected availability of reward elicited significantly higher fluorescence than did expected consumption (Fig. 4, J and K). In the "unexpected reward omission" session, where the US was occasionally omitted after the predictive CS, fluorescence decreased below the pre-CS baseline after the time at which the US would have normally become available after CS presentation (Fig. 4, L and M).

Cellular-level imaging of functionally heterogeneous DA transients in mouse cortex

Finally, we tested whether two-photon imaging with dLight1 could reveal the spatiotemporal release of DA associated with reward in the cortex. The cortex receives projection axons from both SNc and VTA. Inputs from these nuclei carry distinct dopaminergic signals influencing motor control and reward learning, respectively (*10*, *35*). To demonstrate the utility of dLight1 in detecting behavior-related DA signals, we broadly labeled frontal/motor cortex with AAV9.*hSynapsin1*.dLight1.2, followed by two-photon imaging of dLight1-expressing layer 2/3 neurons in head-fixed mice. The animals had fully learned a visuomotor association task that required them to run in response to a visual "Go" cue in order to receive a water reward (Fig. 5, A and B). We observed task-related DA transients, distinguishable from motion artifacts (fig. S15), across cell-sized regions of interest (ROIs) across the field of view (Fig. 5C and fig. S16).

Aligning the DA transients to trial/standstill phase onset, we found two types of task-relevant DA responses during the reward expectation and reward delivery intervals. An average of 63% of responsive ROIs showed significantly increased DA transients that correlated with reward, which were abolished by unexpected reward omission (20% of randomly selected trials) (Fig. 5D, right). A subset of ROIs (~37%) showed significantly increased DA transients that lasted during the short phase of "Go" stimulus presentation for both rewarded and nonrewarded trials (Fig. 5D, left). These transient increases during the stimulus presentation phase were not caused by the stimulus appearance itself, because no significant increase in DA levels was observed during miss trials during which the animal saw the stimulus but did not respond (Fig. 5D, yellow traces).

To investigate whether these early responses shown in 37% of ROIs reflect increased DA levels during reward expectation or correlate with locomotion, we aligned the trials at running onset (Fig. 5E, group averages; fig. S16G, single ROIs) and compared the DA transients of runs triggered by the "Go" stimulus (when the animals expected a reward) with spontaneous runs that erroneously occurred during the standstill phase (with no reward expectation). A small subset of responsive ROIs (5%) showed significant increases in DA transients during reward expectation but not spontaneous running (Fig. 5E, center), whereas the other 32% of ROIs correlated with locomotion (Fig. 5E, left). The 63% of ROIs responsive to reward only (Fig. 5D, right) also showed increased DA transients during the early stimulus presentation phase consisting of both locomotion- and reward expectation–related responses (Fig. 5E, right). All three types of responses were consistently seen across animals. Comparing the heterogeneity of response transients between layer 1 and layers 2/3 of cortical area M1 (fig. S16, E and F), we found that layer 2/3 showed more ROIs active during reward. A similar number of ROIs responded to locomotion and reward expectation in both layers (fig. S16H). Mesocortical dopaminergic projections are thus spatially intermingled, and activation of these inputs leads to spatiotemporally heterogeneous DA signals in the cortex whose dynamics depends on motor behavior, reward expectation, and consumption.

Conclusion

We developed and applied a new class of genetically encoded indicators that overcome major barriers of current methods to permit high-resolution imaging of DA dynamics in acute brain slices and in behaving mice. The submicromolar affinity and fast kinetics of dLight1 offer fast temporal resolution (10 ms on, 100 ms off) to detect the physiologically or behaviorally relevant DA transients with higher molecular specificity relative to existing electrochemical or cell-based probes (*14*). For example, in NAc of freely behaving mice, longitudinal measurements revealed different changes in time-resolved DA signals encoding either predictive cue or reward consumption across learning.

The disparate contributions of synaptic, extrasynaptic, and spillover DA events to circuit function are not addressable without fast, robust, and genetically encoded sensors. In a dorsal striatal slice, dLight1 reliably detected the concentration and time course of DA transients and their modifications by pharmacological compounds. The rapid rise of fluorescence (10 ms) and the peak concentration (10 to 30 μM) of DA after electrical stimulation indicates that the initial measures of DA are closely associated with the site of release (*26*). The decline of fluorescence, particularly in the presence of cocaine, results primarily from reuptake and diffusion of DA away from release sites.

dLight1 also permits measurement of functionally heterogeneous DA transients at the cellular level with high spatial resolution. In the cortex, two-photon imaging with dLight1 revealed a DA transient map with spatially distributed,

functionally heterogeneous DA signals during a visuomotor learning task. Simultaneous calcium imaging can further determine how spatiotemporal differences in DA levels relate to ongoing neural activity and influence associative learning or goal-directed behavior.

dLight1.1 and dLight1.2 are optimized sensor variants that can be immediately applied to ex vivo or in vivo studies, as they offer a good balance between dynamic range and affinity. Other dLight variants may be suitable for measuring synaptic release (dLight1.3) or tonic DA transients (dLight1.4). Given the broadly tunable affinity and dynamic range of dLight1, protein engineering and high-throughput screening efforts can further optimize the signal-to-noise ratio and molecular specificity (*36*) as well as the performance of other neuromodulator indicators.

In combination with calcium imaging and optogenetics, our sensors are well poised to permit direct functional analysis of how the spatiotemporal coding of neuromodulatory signaling mediates the plasticity and function of target circuits.

REFERENCES AND NOTES

1. N. X. Tritsch, B. L. Sabatini, Dopaminergic modulation of synaptic transmission in cortex and striatum. *Neuron* **76**, 33–50 (2012). doi: 10.1016/j.neuron.2012.09.023; pmid: 23040805
2. R. A. Wise, Dopamine, learning and motivation. *Nat. Rev. Neurosci.* **5**, 483–494 (2004). doi: 10.1038/nrn1406; pmid: 15152198
3. J. T. Dudman, J. W. Krakauer, The basal ganglia: From motor commands to the control of vigor. *Curr. Opin. Neurobiol.* **37**, 158–166 (2016). doi: 10.1016/j.conb.2016.02.005; pmid: 27012960
4. W. Schultz, P. Dayan, P. R. Montague, A neural substrate of prediction and reward. *Science* **275**, 1593–1599 (1997). doi: 10.1126/science.275.5306.1593; pmid: 9054347
5. S. H. Lee, Y. Dan, Neuromodulation of brain states. *Neuron* **76**, 209–222 (2012). doi: 10.1016/j.neuron.2012.09.012; pmid: 23040816
6. E. Marder, Neuromodulation of neuronal circuits: Back to the future. *Neuron* **76**, 1–11 (2012). doi: 10.1016/j.neuron.2012.09.010; pmid: 23040802
7. W. Schultz, Dopamine reward prediction-error signalling: A two-component response. *Nat. Rev. Neurosci.* **17**, 183–195 (2016). doi: 10.1038/nrn.2015.26; pmid: 26865020
8. W. X. Pan, R. Schmidt, J. R. Wickens, B. I. Hyland, Dopamine cells respond to predicted events during classical conditioning: Evidence for eligibility traces in the reward-learning network. *J. Neurosci.* **25**, 6235–6242 (2005). doi: 10.1523/JNEUROSCI.1478-05.2005; pmid: 15987953
9. J. Y. Cohen, S. Haesler, L. Vong, B. B. Lowell, N. Uchida, Neuron-type-specific signals for reward and punishment in the ventral tegmental area. *Nature* **482**, 85–88 (2012). doi: 10.1038/nature10754; pmid: 22258508
10. M. W. Howe, D. A. Dombeck, Rapid signalling in distinct dopaminergic axons during locomotion and reward. *Nature* **535**, 505–510 (2016). doi: 10.1038/nature18942; pmid: 27398617
11. G. Cui *et al*., Concurrent activation of striatal direct and indirect pathways during action initiation. *Nature* **494**, 238–242 (2013). doi: 10.1038/nature11846; pmid: 23354054
12. A. Jaquins-Gerstl, A. C. Michael, A review of the effects of FSCV and microdialysis measurements on dopamine release in the surrounding tissue. *Analyst* **140**, 3696–3708 (2015). doi: 10.1039/C4AN02065K; pmid: 25876757
13. M. Ganesana, S. T. Lee, Y. Wang, B. J. Venton, Analytical Techniques in Neuroscience: Recent Advances in Imaging, Separation, and Electrochemical Methods. *Anal. Chem.* **89**, 314–341 (2017). doi: 10.1021/acs.analchem.6b04278; pmid: 28105819
14. A. Muller, V. Joseph, P. A. Slesinger, D. Kleinfeld, Cell-based reporters reveal in vivo dynamics of dopamine and norepinephrine release in murine cortex. *Nat. Methods* **11**, 1245–1252 (2014). doi: 10.1038/nmeth.3151; pmid: 25344639
15. D. Lee *et al*., Temporally precise labeling and control of neuromodulatory circuits in the mammalian brain. *Nat. Methods* **14**, 495–503 (2017). doi: 10.1038/nmeth.4234; pmid: 28369042
16. C. P. Ford, P. E. Phillips, J. T. Williams, The time course of dopamine transmission in the ventral tegmental area. *J. Neurosci.* **29**, 13344–13352 (2009). doi: 10.1523/JNEUROSCI.3546-09.2009; pmid: 19846722
17. C. P. Ford, S. C. Gantz, P. E. Phillips, J. T. Williams, Control of extracellular dopamine at dendrite and axon terminals. *J. Neurosci.* **30**, 6975–6983 (2010). doi: 10.1523/JNEUROSCI.1020-10.2010; pmid: 20484639
18. T. W. Chen *et al*., Ultrasensitive fluorescent proteins for imaging neuronal activity. *Nature* **499**, 295–300 (2013). doi: 10.1038/nature12354; pmid: 23868258
19. J. S. Marvin *et al*., An optimized fluorescent probe for visualizing glutamate neurotransmission. *Nat. Methods* **10**, 162–170 (2013). doi: 10.1038/nmeth.2333; pmid: 23314171
20. A. Manglik *et al*., Structural Insights into the Dynamic Process of β2-Adrenergic Receptor Signaling. *Cell* **161**, 1101–1111 (2015). doi: 10.1016/j.cell.2015.04.043; pmid: 25981665
21. S. G. Rasmussen *et al*., Crystal structure of the β2 adrenergic receptor-Gs protein complex. *Nature* **477**, 549–555 (2011). doi: 10.1038/nature10361; pmid: 21772288
22. C. D. Strader *et al*., Conserved aspartic acid residues 79 and 113 of the beta-adrenergic receptor have different roles in receptor function. *J. Biol. Chem.* **263**, 10267–10271 (1988). pmid: 2899076
23. R. Irannejad *et al*., Conformational biosensors reveal GPCR signalling from endosomes. *Nature* **495**, 534–538 (2013). doi: 10.1038/nature12000; pmid: 23515162
24. R. G. Vickery, M. von Zastrow, Distinct dynamin-dependent and -independent mechanisms target structurally homologous dopamine receptors to different endocytic membranes. *J. Cell Biol.* **144**, 31–43 (1999). doi: 10.1083/jcb.144.1.31; pmid: 9885242
25. J. T. Yorgason, D. M. Zeppenfeld, J. T. Williams, Cholinergic Interneurons Underlie Spontaneous Dopamine Release in Nucleus Accumbens. *J. Neurosci.* **37**, 2086–2096 (2017). doi: 10.1523/JNEUROSCI.3064-16.2017; pmid: 28115487
26. N. A. Courtney, C. P. Ford, The timing of dopamine- and noradrenaline-mediated transmission reflects underlying differences in the extent of spillover and pooling. *J. Neurosci.* **34**, 7645–7656 (2014). doi: 10.1523/JNEUROSCI.0166-14.2014; pmid: 24872568
27. A. A. Mamaligas, Y. Cai, C. P. Ford, Nicotinic and opioid receptor regulation of striatal dopamine D2-receptor mediated transmission. *Sci. Rep.* **6**, 37834 (2016). doi: 10.1038/srep37834; pmid: 27886263
28. L. A. Gunaydin *et al*., Natural neural projection dynamics underlying social behavior. *Cell* **157**, 1535–1551 (2014). doi: 10.1016/j.cell.2014.05.017; pmid: 24949967
29. K. R. Tan *et al*., GABA neurons of the VTA drive conditioned place aversion. *Neuron* **73**, 1173–1183 (2012). doi: 10.1016/j.neuron.2012.02.015; pmid: 22445344
30. F. Brischoux, S. Chakraborty, D. I. Brierley, M. A. Ungless, Phasic excitation of dopamine neurons in ventral VTA by noxious stimuli. *Proc. Natl. Acad. Sci. U.S.A.* **106**, 4894–4899 (2009). doi: 10.1073/pnas.0811507106; pmid: 19261850
31. H. Dana *et al*., Sensitive red protein calcium indicators for imaging neural activity. *eLife* **5**, e12727 (2016). doi: 10.7554/eLife.12727; pmid: 27011354
32. S. A. Taha, H. L. Fields, Encoding of palatability and appetitive behaviors by distinct neuronal populations in the nucleus accumbens. *J. Neurosci.* **25**, 1193–1202 (2005). doi: 10.1523/JNEUROSCI.3975-04.2005; pmid: 15689556
33. J. J. Day, M. F. Roitman, R. M. Wightman, R. M. Carelli, Associative learning mediates dynamic shifts in dopamine signaling in the nucleus accumbens. *Nat. Neurosci.* **10**, 1020–1028 (2007). doi: 10.1038/nn1923; pmid: 17603481
34. J. J. Clark *et al*., Chronic microsensors for longitudinal, subsecond dopamine detection in behaving animals. *Nat. Methods* **7**, 126–129 (2010). doi: 10.1038/nmeth.1412; pmid: 20037591
35. J. A. da Silva, F. Tecuapetla, V. Paixão, R. M. Costa, Dopamine neuron activity before action initiation gates and invigorates future movements. *Nature* **554**, 244–248 (2018). doi: 10.1038/nature25457; pmid: 29420469
36. K. D. Piatkevich *et al*., A robotic multidimensional directed evolution approach applied to fluorescent voltage reporters. *Nat. Chem. Biol.* **14**, 352–360 (2018). doi: 10.1038/s41589-018-0004-9

ACKNOWLEDGMENTS

We thank B. P. McGrew for assistance during in vitro sensor library screening; H. Cheng for producing AAV virus; L. Lavis (Janelia Research Campus) for providing NV-caged DA; E. Carey for performing cortical viral vector injections; and B. Mensh for critical advice in writing and revising the manuscript. This project was made possible with generous help from L. Looger (Janelia Research Campus). **Funding:** Supported by NIH BRAIN Initiative U01NS090604 and U01NS013522, DP2MH107056 (L.T.); DP2NS083038, R01NS085938, P30CA014195 (A.N.); BRAIN Initiative U01NS013522 (J.T.W. and M.v.Z.); BRAIN Initiative U01NS094247 and R01NS104944 (H.Z.); NIH 1R01MH110556 (D.D.); and NIH DP2NS087949, NIH/NIA R01AG047664 (V.G.). K.M. is a DFG research fellow and recipient of a Catharina Foundation postdoctoral scholar award. V.G. is a Heritage Principal Investigator supported by the Heritage Medical Research Institute. **Author contributions:** L.T. and T.P. conceived the project; T.P. and L.T. designed, screened, and optimized sensors and characterized them in mammalian cells and cultured neurons; R.L. simulated the structure of the sensor; A.M. and M.v.Z. characterized signaling properties of the sensor; W.-H.X. and H.Z. characterized the sensor in organotypic brain slices; J.T.W. performed characterization in acute brain slices; M.W.H. and D.D. characterized the sensor in vivo in the dorsal striatum; J.R.C. and V.G. performed fiber photometry recordings coupled with optogenetic manipulations, calcium imaging, and behavioral experiments in NAc, analyzed the data, and prepared the related figures and text; M.J.J. performed hybridization chain reaction experiments and prepared relevant figures and text with input from J.R.C. and V.G.; K.M., R.W.F., and A.N. performed the two-photon imaging experiments in the cortex of behaving mice, analyzed the data, and prepared the related figures and text; all authors analyzed the data; L.T. led the project; and L.T. and T.P. wrote the paper with contributions from all authors. **Competing interests:** L.T., R.L., and T.P. have submitted a provisional patent application on sensor engineering. **Data and materials availability:** All DNA and viruses have been deposited in NCBI (accession number MH244549-MH244561), ADDGENE, and the University of Pennsylvania Vector Core. All DNA plasmids and viruses are available from UC Davis or designated repository under a material transfer agreement. Computer codes are deposited in github (https://github.com/GradinaruLab/dLight1/). All other data needed to evaluate the conclusion in the paper are present in the paper or the supplementary materials.

SUPPLEMENTARY MATERIALS

www.sciencemag.org/content/360/6396/eaat4422/suppl/DC1
Materials and Methods
Figs. S1 to S16
Data S1 to S3
References (*37*–*67*)

4 March 2018; accepted 17 May 2018
Published online 31 May 2018
10.1126/science.aat4422